The comparative behavior of apatite-zircon U-Pb systems in Apollo 14 breccias: Implications for the thermal history of the Fra Mauro Formation

A. A. NEMCHIN[1]*, R. T. PIDGEON[1], D. HEALY[1], M. L. GRANGE[1], M. J. WHITEHOUSE[2], and J. VAUGHAN[1]

[1]Department of Applied Geology, Curtin University of Technology, Bentley, Western Australia, 6102, Australia
[2]Swedish Museum of Natural History, Box 50007, SE-104 05 Stockholm, Sweden
*Corresponding author. E-mail: nemchina@kalg.curtin.edu.au

Abstract–We report secondary ion mass spectrometry (SIMS) U-Pb analyses of zircon and apatite from four breccia samples from the Apollo 14 landing site. The zircon and apatite grains occur as cogenetic minerals in lithic clasts in two of the breccias and as unrelated mineral clasts in the matrices of the other two. SIMS U-Pb analyses show that the ages of zircon grains range from 4023 ± 24 Ma to 4342 ± 5 Ma, whereas all apatite grains define an isochron corresponding to an age of 3926 ± 3 Ma. The disparity in the ages of cogenetic apatite and zircon demonstrates that the apatite U-Pb systems have been completely reset at 3926 ± 3 Ma, whereas the U-Pb system of zircon has not been noticeably disturbed at this time. The apatite U-Pb age is slightly older than the ages determined by other methods on Apollo 14 materials highlighting need to reconcile decay constants used for the U-Pb, Ar-Ar and Rb-Sr systems. We interpret the apatite age as a time of formation of the Fra Mauro Formation. If the interpretation of this Formation as an Imbrium ejecta is correct, apatite also determines the timing of Imbrium impact. The contrast in the Pb loss behavior of apatite and zircon places constraints on the temperature history of the Apollo 14 breccias and we estimate, from the experimentally determined Pb diffusion constants and an approximation of the original depth of the excavated samples in the Fra Mauro Formation, that the breccias experienced an initial temperature of about 1300–1100 °C, but cooled within the first five to ten years.

INTRODUCTION

Zircon U-Pb geochronology has already made an important contribution to the understanding of lunar evolution (Compston et al. 1984a; Meyer et al. 1996; Pidgeon et al. 2007; Nemchin et al. 2008). However, the U-Pb system of lunar apatite has rarely been used despite its potential for dating lunar events, especially as apatite (together with merrillite) is widely available in lunar rocks compared to zircon, which appears to be restricted to rocks that carry a KREEP signature. Whereas the use of apatite will increase the pool of lunar rocks available for U-Pb dating its relatively low U concentration and generally high content of initial Pb present significant problems for achieving precise age measurements. In recent years, the SHRIMP group in Hiroshima have investigated phosphates in a number extraterrestrial materials including lunar meteorites (e.g., Terada and Sano 2003; Terada et al. 2007). Results have shown that it is possible to extract meaningful ages from the apatite and merrillite contained in lunar rocks, but the

relatively large errors of about 100 Ma inhibit the resolution of small scale age variations. However, increased counting times on all isotopes, used in this study, as described below, has greatly improved the analytical precision allowing meaningful comparisons of apatite ages with those from other techniques.

The low closure temperature (typically estimated as 450–500 °C, e.g., Cherniak et al. 1991; Krogstad and Walker 1994; Chamberlain and Bowring 2000) of the U-Pb system makes apatite susceptible to isotopic disturbance or resetting during meteoritic bombardment. While this could introduce ambiguities in the interpretation of the U-Pb results the large difference in thermal stability of apatite and zircon provides an opportunity to better resolve the impact and possibly thermal history of the Moon. The purpose of present study was to make use of the contrasting behavior of the two U-Pb systems by investigating the U-Pb age patterns of co-existing zircons and apatites from the same samples of lunar breccias from Apollo 14 landing site. The aims were to investigate the geochronological possibilities of apatite and the implications

of the ages for understanding the conditions of formation of the host breccias and the Fra Mauro Formation.

APOLLO 14 SAMPLES

The objective of Apollo 14 mission was to sample material ejected from the Imbrium basin. The landing site was an area of low rounded hills covered by regolith with a scattering of boulders, with the larger boulders concentrated near the rim of the nearby Cone crater. It has been proposed that, at the landing site, the regolith, with a depth of 5–12 m (Eggleton and Offield 1970) or 10–20 m (Swan et al. 1971), overlays the Fra Mauro Formation, interpreted as representing the Imbrium basin ejecta sheet, with an estimated thickness of 100–200 m (Wilhems 1987). The presence of boulders, including complex fragmental breccias, impact-melt breccias and clast-poor impact melts with generally basaltic and KREEP–rich compositions at the surface (Hiesinger and Head 2006) has been attributed to ejection of Fra Mauro Formation material during impact formation of the 25 Ma old Cone crater (Turner et al. 1971; Wilhelms 1987). However, Heisinger and Head (2006) comment "that it is still unclear which Apollo 14 samples represent true Imbrium ejecta and which represent locally derived materials." While the question of the ultimate source of the boulders has implications for the interpretation of geochronological results, the consistent ^{40}Ar-^{39}Ar ages determined on whole rocks and fines (Turner et al. 1971, 1972; Kirsten et al. 1972; Alexander and Davis 1974) and Rb-Sr ages on whole rock samples from Apollo 14 (Papanastassiou and Wasserburg 1971; Compston et al. 1972) of about 3.87 Ga, have been interpreted as dating formation of the Imbrium basin (Wilhelms 1987; Stöffler and Ryder 2001). This age contrasts with SIMS determined U-Pb ages of zircons from Apollo 14 breccias, which range from about 4.00 Ga to 4.40 Ga with distinct age peaks at 4.35 Ga and 4.20 Ga (Meyer et al. 1996; Nemchin et al. 2008), demonstrating that materials from the Fra Mauro breccias have a significantly older, pre-Imbrium history. Whereas temperature and shock associated with formation of the Fra Mauro Formation were sufficient to reset the ^{40}Ar-^{39}Ar and Rb-Sr ages, the zircon ages show that these conditions were not of sufficient intensity to disturb the zircon U-Pb systems. To further advance this understanding we have determined U-Pb ages of apatite and zircon from four breccias, including a norite clast (thin section 14306,60), an anorthosite clast (thin section 14321,16) and two examples (14066,47; 14303,52) of unrelated but closely spaced zircon and apatite clasts in the matrix of the same breccia.

In the breccia thin sections zircon and apatite co-exist on the scale of less than one centimeter and as a consequence, have experienced a common PT and transport history during formation of the breccia. The PT conditions may not have been uniform for all breccias in the Apollo 14 sampled area

and to investigate this we have made SIMS measurements on zircon and apatite grains from breccia sample 14321 taken from a large boulder in the vicinity of Cone crater and samples 14306, 14066 and 14303 from boulders about one kilometer to the south west in the vicinity of the Lunar Module. To investigate the possibility of partial Pb loss the internal consistency of the U-Pb systems of many grains have been tested by making more than one SIMS measurement on a number of the apatite and zircon crystals. The following presents a brief description of the analytical methods, followed by a description of SIMS U-Pb analytical results for zircon and apatite grains from each studied thin section, and discussion of the implications of these results for lunar impact history and the thermal conditions during deposition of the Fra Mauro Formation.

ANALYTICAL TECHNIQUE

Polished thin sections 14306,60, 14066,47 14303,52 and 14321,16 were systematically searched using SEM/EDS to locate grains of apatite and zircon, which were identified using a combination of BSE grey-scale images and semi-quantitative EDS analysis. U-Pb analyses on zircons and apatites in the first two samples were made using the Western Australian consortium SHRIMP II at Curtin University of Technology. The other two samples were analyzed using CAMECA IMS 1270 ion probe in Stockholm.

SHRIMP analyses of zircon grains were made using procedure described by Compston et al. (1984a) and Kennedy and de Laeter (1994). Analyses of apatite followed similar protocol, but integration times have been increased 3–4 times for Pb and U isotopes in order to increase the total number of collected counts. The SIMS methodology used at the Nordsim facility closely followed previously published analytical descriptions (Whitehouse et al. 1999; Whitehouse and Kamber 2005; Nemchin et al. 2008).

U/Pb ratios in zircons were calibrated against the Sri-Lankan zircon CZ3 (Pidgeon et al. 1994). Initial data reduction was made using SQUID (Ludwig 2001) for SHRIMP analyses and in-house developed software at Nordsim for the IMS 1270 analyses.

A large apatite crystal with an age of 2058 Ma and U concentration of 67 ppm was used as the reference during all analytical sessions both on SHRIMP and IMS 1270. U/Pb ratios in lunar apatite grains were calibrated using linear relationships in the Ln(^{206}Pb/^{238}U) versus Ln(^{238}U^{16}O/^{238}U) coordinates. It is difficult to establish the slopes of the lines for individual ion probe sessions as the variation of ^{238}U^{16}O/^{238}U is very small (Fig. 1a). However, all standard analyses combined define a slope of 1.80. The variation of ^{238}U^{16}O/^{238}U in the lunar apatites is about five times larger than that of the standard, which is probably a consequence of the thin
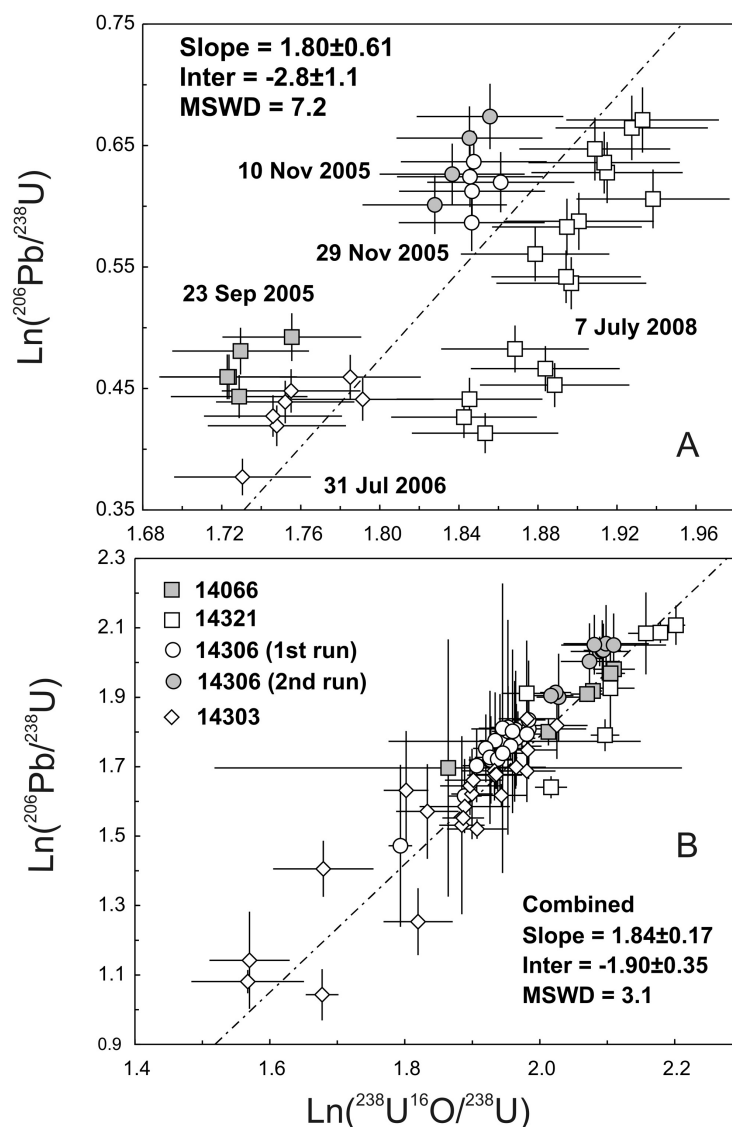
Fig. 1. U-Pb calibration lines for SIMS analyses of apatite. a) Analyses of 2058 Ma apatite used as a reference material. b) All analyses of lunar samples whose combined slope of 1.84 ± 0.17 has been used to correct Pb/U in all lunar apatite analyses.

sections having less perfect surfaces than the standard grain mount. Data collected during five ion probe sessions have a combined slope of 1.84 ± 0.17 (Fig. 1b). This slope was used to correct Pb/U in all lunar apatite analyses.

All errors of individual analyses are presented at 2-sigma level (SD), whereas the average ages are calculated as 95% confidence limit.

Common Pb Correction
(Analysis of Olivine from the Breccia Sample 14321,16)

The initial Pb correction of lunar samples is complicated by the highly radiogenic Pb compositions of many lunar rocks (e.g., Gale 1972; Tera and Wasserburg 1972). Meyer et al. (1996) used a model where the initial Pb selected for the correction was calculated as a mixture of meteoritic Pb

(assumed to be similar to Canyon Diablo troilite Pb) and radiogenic lunar Pb determined in feldspars from the felsic clasts found in lunar breccias (Compston et al. 1991). However, Nemchin et al. (2008) suggested that most of [204]Pb in the lunar samples is a result of contamination with the terrestrial Pb, most likely originated from the cutting and polishing of the samples. To investigate the question of initial Pb correction further we have analyzed isotopic composition of Pb in an olivine clast from the sample 14321,16 in the assumption that olivine would not contain original lunar Pb. The analyses were made using the Cameca IMS 1270 at Nordsim operating in static multi-collector configuration using four ion-counting electron multipliers. The data were accumulated during 40 cycles with 30 s integration during each cycle. Relative detector efficiencies were calibrated using measurements of basalt glass BCR-2 (Woodhead and

Table 1. Isotopic composition of Pb in olivine from the sample 14321,16.

Spot	^{206}Pb (cps[*])	$^{206}Pb/^{204}Pb$	%err	$^{207}Pb/^{204}Pb$	%err	$^{208}Pb/^{204}Pb$	%err
Ol-1	16.1	18.03	3.1	15.33	3.1	36.94	3.0
Ol-2	1316.8	18.16	0.3	15.79	0.3	37.70	0.3
Ol-3	1699.8	18.16	0.3	15.85	0.3	37.69	0.3
Average		18.12 ± 0.15		15.66 ± 0.57		37.44 ± 0.87	
		(Single stage Stacey and Kramers model age = 493 Ma)					

[*]Counts per second.

Hergt 2000). The results (Table 1) indicate the presence of a variable but significant proportion of Pb in the olivine despite cleaning the sample surface before gold coating and pre-spattering each spot before analysis. The measured isotopic compositions are also consistent with the terrestrial origin of Pb giving single stage Stacey and Kramers model ages (Stacey and Kramers 1975) ranging between about −160 and 800 Ma. Consequently all analyses of lunar samples in this study have been corrected using an average composition of Pb determined from the analyses of olivine.

SAMPLES AND ANALYTICAL RESULTS

Breccia Thin Section 14306,60

Sample 14306 is classified as a crystalline matrix breccia (Simonds et al. 1977). Polished thin section 14306,60 contains one large fragment (5 × 4 mm) of noritic gabbro microbreccia which consists of coarse-grained aggregates and broken crystal fragments (up to 1 mm) of plagioclase and pyroxene set in a dark glassy matrix (Fig. 2a). This fragment appears to represent a single rock clast that has been broken into several pieces that have rotated against each other before consolidating together again in the breccia matrix. This partly broken plagioclase-pyroxene clast contains numerous apatite, zircon and ilmenite grains ranging in size up to 0.7 mm for the largest apatite and 0.4 mm for the largest zircon. Apatite and zircon grains vary from euhedral crystals in the better preserved pieces of the original clast (Fig. 2b) to broken fragments in the more broken parts of the norite.

Single SIMS analyses of seven zircon grains were obtained from the sample 14306,60. All seven analyses uncorrected for common Pb contribution fall on a line in the 3D $^{207}Pb/^{206}Pb - ^{204}Pb/^{206}Pb - ^{238}U/^{206}Pb$ system with MSWD of 1.5. This line defines an initial $^{206}Pb/^{204}Pb$ of 17.4 ± 4.3 and initial $^{207}Pb/^{204}Pb$ of 14.7 ± 3.2. When corrected for the common Pb obtained from the analyses of olivine all analyses fall on the concordia curve in the $^{207}Pb/^{206}Pb - ^{238}U/^{206}Pb$ plain and define an age of 4203 ± 7 Ma (Fig. 3), while the weighted average of $^{207}Pb/^{206}Pb$ common Pb corrected ages is 4201 ± 6 Ma. These ages are similar to the age of 4203 ± 25 Ma determined for a zircon grain from the same thin section by Compston et al. (1984b) and we interpret them as dating crystallization of the norite which includes the cogenetic apatite.

SIMS U-Pb measurements were made on nine apatite grains from this thin section (Table 2). At least two analyses were made on each grain. Compared to other analyzed samples, all grains from 14306,60 show low U concentrations between 20 and 44 ppm and a variable Th/U between 9.7 and 26.8. The relatively low U content is accompanied by a high proportion of common Pb, with $^{206}Pb/^{204}Pb$ from 31 to above 300. The high common Pb, combined with the apparent homogeneity of individual apatite grains, results in relatively imprecise ages calculated for these grains (Table 3). When combined on a 3D-concordia plot the intercept with concordia in the $^{238}U/^{206}Pb - ^{207}Pb/^{206}Pb - ^{204}Pb/^{206}Pb$ coordinates gives an age of 3865 ± 110 Ma (Fig. 4), while the $^{204}Pb/^{206}Pb - ^{207}Pb/^{206}Pb$ isochron age for the same data set is 3944 ± 24 Ma (Fig. 5) and the weighted average of the common Pb corrected $^{207}Pb/^{206}Pb$ age is 3918 ± 14 Ma.

Breccia Thin Section 14066,47

Sample 14066 is classified as a crystalline matrix breccia (Simonds et al. 1977) with medium grey lithic fragments in a pale grey matrix. Polished thin section 14066,47 consists of subhedral to euhedral single crystals and broken fragments of plagioclase and pyroxene (up to 1.4 mm) together with a few rounded, darker grey, fine-grained lithic fragments (up to 1 mm) set in a fine-grained, pale grey, plagioclase-rich matrix. Some of the rounded lithic fragments are surrounded by narrow, highly birefringent reaction rims. The section contains numerous grains of apatite, zircon and ilmenite disseminated through the fine-grained matrix. The largest apatite grain is about 100 mm and the largest zircon grain is about 200 mm in size. However, most of these grains are 10 to 20 μm in diameter, and only a few were large enough for ion microprobe analysis.

Five zircon grains analyses (Table 2) fall into three distinctly different age groups when initial Pb uncorrected data are plotted on Tera-Wasserburg diagram (Fig. 6). Analyses of three grains define a single line in the 3D $^{207}Pb/^{206}Pb - ^{204}Pb/^{206}Pb - ^{238}U/^{206}Pb$ system with a concordia intercept age of 4155 ± 20 Ma (MSWD = 3.1). Similar age of 4158 ± 19 Ma (MSWD=3.3) can be determined by averaging common Pb corrected $^{207}Pb/^{206}Pb$ for these analyses. SIMS U-Pb analyses for two other grains are concordant and have common Pb corrected $^{207}Pb/^{206}Pb$ ages of 4352 ± 6 Ma and 4225 ± 18 Ma.
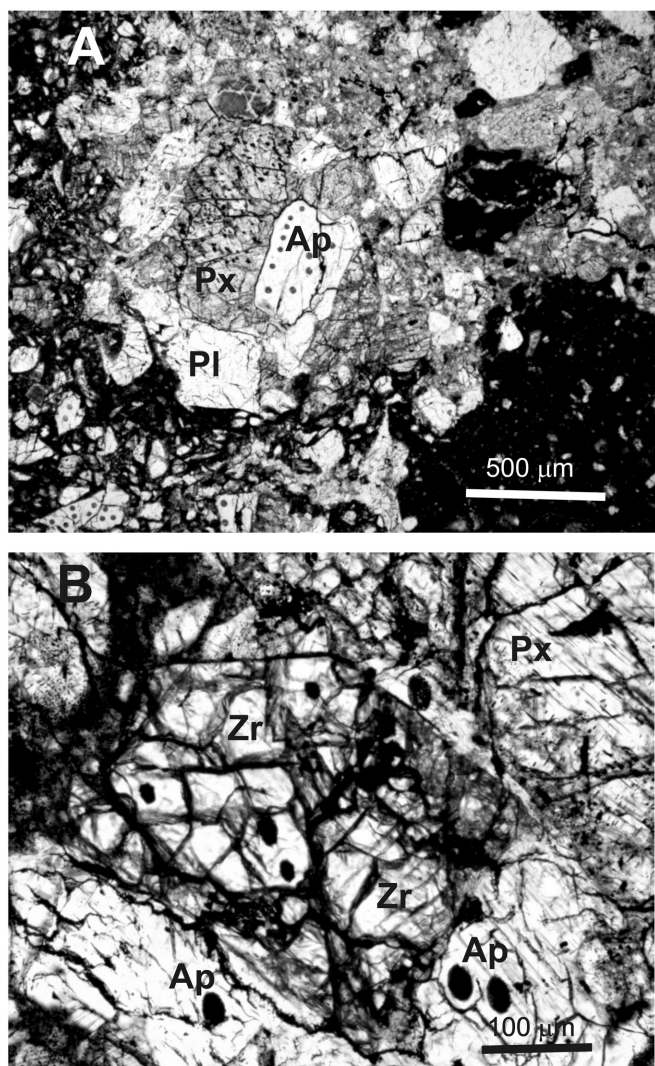
Fig. 2. Analyzed zircon and apatite grains from the noritic gabbro clast in the breccia thin section 14306, 60 (plane polarized light); a) fragment of the noritic gabbro clast surrounded by the dark matrix; b) zircon and apatite crystals surrounded by the pyroxene grains inside the noritic gabbro clast. Px, pyroxene; Pl, plagioclase; Ap, apatite; Zr, zircon.

Seven analyzed apatite grains show a range of U and Th contents and Th/U ratios indicating they are independent crystals possibly of different primary ages as are the zircons in the matrix. Also, the variation of $^{206}Pb/^{204}Pb$ between 930 and 8583 makes the results insensitive to the common Pb correction. The $^{207}Pb/^{206}Pb$ ages range of the seven grains is 3916 ± 6 to 3939 ± 9 Ma. These ages are significantly younger than the ages of co-existing zircons. The 3D-concordia intercept in the $^{238}U/^{206}Pb–^{207}Pb/^{206}Pb–^{204}Pb/^{206}Pb$ coordinates of the apatite data gives an age of 3915 ± 17 Ma (Fig. 4), while $^{204}Pb/^{206}Pb–^{207}Pb/^{206}Pb$ isochron age for the same data set is 3919 ± 18 Ma (Fig. 5) and the weighted average of the common Pb corrected $^{207}Pb/^{206}Pb$ age is 3925 ± 7 Ma.
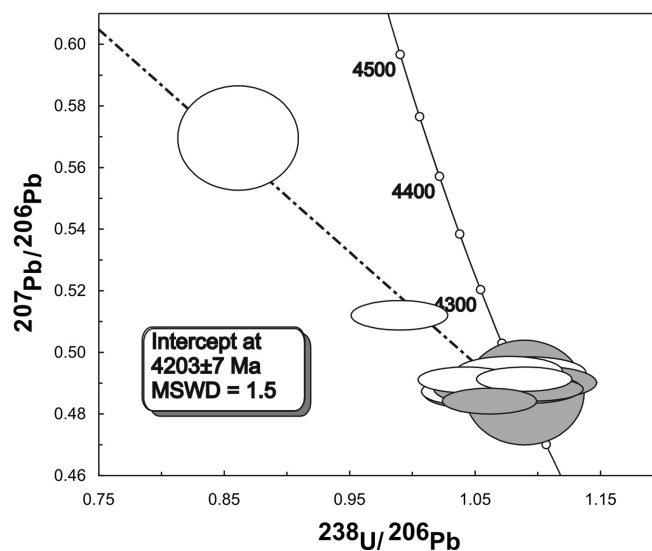
Fig. 3. Tera-Wasserburg concordia diagram showing analyses of zircon from the noritic gabbro clast found in the thin section 14306,60. Open ellipses, data uncorrected for common Pb; grey ellipses, data corrected for the common Pb obtained from the analysis of olivine.

Breccia Thin Section 14303,52

Sample 14303 is classified as polymict breccia with a holocrystalline matrix enclosing lithic, plagioclase and rare olivine and pyroxene fragments (Carlson et al. 1978). Section 14303,52 contains a population of crystal clasts dominated by plagioclase, pyroxene, olivine and a minor opaque mineral. Some norite, pyroxene and olivine rich clasts and older generation breccias are also present in the section. Ten apatite grains ranging in size between 50 and 200 μm have been found in the breccia matrix. One zircon is incorporated into a ~1–1.5 mm Ol-Px rich lithic clast, while two others are found in smaller 0.2–0.3 mm Px and Px-Pl aggregates. The remaining six zircon grains are contained in the breccia matrix.

Thirteen analyses of the nine zircons from the sample 14303,52 (Table 2) show a range of $^{206}Pb/^{204}Pb$ varying from 121 to 5668 supporting conclusion that the surface of this sample has the higher level of contamination of the group of four analyzed sections, which is also evident in the apatite analyses. U and Th concentrations ranging from 41 to 305 ppm and 27 to 418, respectively, are similar to zircon grains from the sample 14066,47. The range of ages displayed by zircons in these two samples is also similar with exception of one grain (Table 2) that shows a common Pb corrected $^{207}Pb/^{206}Pb$ age of 4002 ± 8 Ma. However, the analysis is strongly reversely discordant and it is difficult to determine how reliable it is (group-1, Fig. 7). The remaining twelve analyses fall broadly into two age groups (Fig. 7). The older group includes five analyses on the grains-2, -5 and -6 and one of two analyses of grain-3. These analyses show a
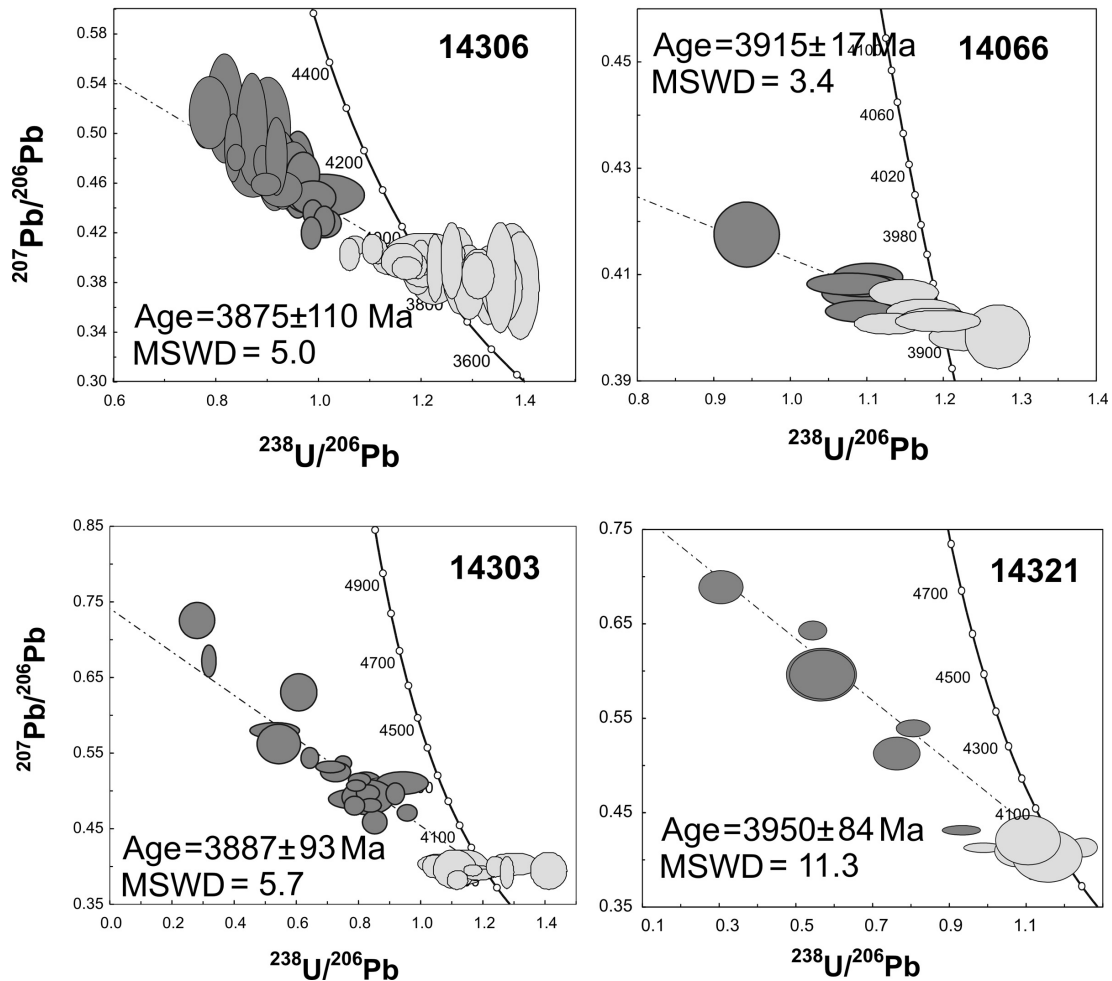
Fig. 4. Projection of 3D $^{207}Pb/^{206}Pb$–$^{204}Pb/^{206}Pb$–$^{238}U/^{206}Pb$ apatite data for all analyzed samples on to Tera-Wasserburg concordia plane. Dark grey ellipses, orthogonal projection of common Pb uncorrected data; light grey ellipses, data projected along the best fit lines (projections of these lines are shown on the diagrams).

range of common Pb corrected $^{207}Pb/^{206}Pb$ ages between 4342 ± 5 Ma and 4306 ± 7 Ma (Table 2). However, even this spread is slightly larger than that expected for a single population and therefore a single age cannot be calculated for this group. The younger analyses show an even larger spread between 4208 ± 4 Ma and 4103 ± 17 Ma (Table 2). It is important to note that, while three analyses of the grain-5 and two analyses of grain-4 show internal consistency falling into the older and younger group respectively, two analyses of grain-3 appear to fall into two different age groups (Table 2), suggesting that the younger group may represent a resetting of 4.34 Ga grains during a secondary event.

SIMS analyses were made on eight apatite grains from this breccia. Common Pb is uniformly higher in apatites from this section compared to the other samples. Three analyses were made on the grain-2 and five on the grains-4, 5 and 7. Analyses show a relatively narrow range of U and Th concentrations determined by the slight difference between the grains rather than internal within-grain variations (e.g., U

content in grain-4 varies from 49 to 64 ppm, and in grain-5 from 29 to 42 ppm). The ages of individual grains with multiple analyses are uniform within the errors (Table 2). When combined all analyses give 3D-concordia intercept of 3887 ± 93 Ma (Fig. 4), $^{204}Pb/^{206}Pb$–$^{207}Pb/^{206}Pb$ isochron age of 3898 ± 33 Ma (Fig. 5) and weighted average of the common Pb corrected $^{207}Pb/^{206}Pb$ age of 3858 ± 16 Ma, indicating that the apatites are significantly younger and more uniform in age than zircons from the same breccia sample.

Breccia Thin Section 14321,16

Sample 14321 was classified as a crystalline matrix breccia (Simonds et al. 1977) with about 30% clasts representing a variety of rock types and older generation microbreccias. The majority of non-breccia clasts are aluminous basalts with only small number of pristine plutonic rocks preserved in the sample. Two zircon and five apatite grains were identified within a single anorthosite clast in thin

Table 2. U-Pb data for the apatite and zircon grains from Apollo 14 breccia thin sections.

Sample	204Pb/206Pb	%err	207Pb/206Pb	%err	208Pb/206Pb	%err	%com Pb[b]	U (ppm)	Th (ppm)	Th/U	207Pb/206Pb age	238U/206Pb	%err	238U/206Pb*[c]	%err	207Pb*/206Pb*	%err
Apatite 14306,60																	
32-1	0.0118	26	0.4916	5.3	3.845	4.1	21.5	23	483	21.7	3862±188	0.866	2.9	1.103	7.8	0.3877	12.5
32-2	0.0090	29	0.4737	4.4	3.695	2.9	16.4	27	522	19.7	3894±141	0.911	2.8	1.089	6.3	0.3960	9.4
32-3	0.0090	27	0.4720	4.1	3.741	2.6	16.3	26	507	20.4	3886±134	0.870	4.5	1.041	7.0	0.3940	8.9
32-4	0.0071	37	0.4611	4.2	4.002	3.0	12.9	24	491	21.3	3911±131	0.913	2.7	1.048	6.2	0.4005	8.7
32-5	0.0059	37	0.4507	3.3	4.615	1.1	10.7	22	501	23.0	3910±104	0.969	4.0	1.085	6.0	0.4003	6.9
56-1	0.0135	11	0.5068	3.0	2.543	1.1	24.6	38	491	13.5	3864±102	0.776	2.5	1.029	4.3	0.3881	6.8
56-2	0.0047	42	0.4410	2.9	2.902	1.9	8.5	34	472	14.5	3913±90	1.002	2.7	1.094	4.8	0.4011	6.0
56-3	0.0122	39	0.5038	6.7	2.312	2.9	22.1	44	417	9.7	3907±261	0.900	3.9	1.156	11.9	0.3994	17.4
56-1	0.0148	35	0.5199	6.9	3.624	7.2	26.9	24	488	20.9	3874±306	0.814	3.7	1.113	13.4	0.3909	20.3
56-2	0.0080	52	0.4666	6.1	3.585	4.4	14.6	26	485	18.9	3899±208	0.958	2.8	1.122	9.3	0.3974	13.8
57-1	0.0319	16	0.6424	4.9	3.266	8.7	57.9	20	511	26.2	3605±587	0.460	4.2	1.093	22.4	0.3275	38.2
57-2	0.0093	34	0.4692	5.3	4.851	3.6	16.9	23	585	26.8	3862±178	0.929	2.9	1.117	7.6	0.3877	11.8
71-1	0.0050	43	0.4501	3.1	2.691	1.3	9.0	30	397	13.5	3940±95	1.009	6.3	1.109	7.7	0.4083	6.3
71-2	0.0101	18	0.4893	2.4	2.687	1.9	18.3	31	425	14.1	3924±90	0.917	2.7	1.122	4.9	0.4040	6.0
71-3	0.0105	5	0.4887	1.6	2.731	0.8	19.0	30	422	14.4	3905±41	0.889	2.8	1.097	3.0	0.3988	2.7
66-1	0.0146	26	0.5165	4.6	3.550	4.2	26.5	23	470	20.7	3864±217	0.785	4.2	1.069	10.2	0.3882	14.4
66-2	0.0124	40	0.5032	7.3	3.507	5.1	22.5	26	496	19.6	3895±281	0.868	2.9	1.121	12.0	0.3962	18.7
7-1	0.0092	20	0.4741	3.3	3.755	2.0	16.7	31	591	19.9	3888±104	0.949	2.7	1.139	4.9	0.3944	6.9
7-2	0.0079	29	0.4666	3.1	3.882	2.3	14.3	32	643	20.5	3906±111	0.968	2.7	1.129	5.6	0.3992	7.4
7-3	0.0056	34	0.4479	2.5	3.766	2.1	10.1	34	642	19.5	3910±85	0.987	3.7	1.098	5.3	0.4003	5.7
7-4	0.0032	49	0.4275	2.2	3.488	1.4	5.7	37	627	17.7	3911±67	1.010	2.6	1.072	3.9	0.4005	4.4
73-1	0.0017	63	0.4254	1.6	2.657	0.9	3.0	36	477	13.6	3951±43	1.001	1.7	1.033	2.6	0.4114	2.9
73-2	0.0079	30	0.4765	2.3	2.547	1.5	14.3	36	470	13.3	3948±100	0.889	1.6	1.037	5.3	0.4106	6.7
73-3	0.0032	43	0.4359	1.9	2.573	1.1	5.8	38	477	13.1	3943±58	0.987	1.6	1.048	3.1	0.4091	3.9
73-4	0.0101	31	0.4882	4.6	2.535	1.2	18.3	37	481	13.5	3919±163	0.831	1.6	1.017	7.2	0.4026	10.8
73-5	0.0091	9	0.4804	1.8	2.610	1.5	16.5	34	456	13.9	3922±49	0.837	1.7	1.002	2.5	0.4034	3.3
73-6	0.0024	69	0.4292	2.3	2.630	2.0	4.3	38	486	13.3	3944±67	1.009	1.7	1.054	3.5	0.4095	4.4
68-1	0.0060	31	0.4548	2.6	2.944	1.9	10.9	34	518	15.7	3924±84	0.925	3.6	1.038	5.2	0.4039	5.6
68-2	0.0087	40	0.4813	5.3	2.956	2.1	15.8	35	531	15.5	3939±173	0.916	1.9	1.089	7.7	0.4079	11.6
34-1	0.0018	61	0.4197	2.5	2.617	1.7	3.3	40	511	13.2	3924±56	0.984	1.7	1.018	2.7	0.4041	3.7
34-2	0.0070	6	0.4587	1.6	2.662	1.6	12.7	38	505	13.8	3904±36	0.895	2.6	1.026	2.8	0.3987	2.4

Table 2. *Continued.* U-Pb data for the apatite and zircon grains from Apollo 14 breccia thin sections.

Sample	$^{204}Pb/$ ^{206}Pb	%err	$^{207}Pb/$ ^{206}Pb	%err	$^{208}Pb/$ ^{206}Pb	%err	%com Pb^b	U (ppm)	Th (ppm)	Th/U	$^{207}Pb/$ ^{206}Pb age	$^{238}U/$ ^{206}Pb	%err	$^{238}U/$ $^{206}Pb^{*C}$	%err	$^{207}Pb^*/$ $^{206}Pb^*$	%err
14066,47																	
69-1	0.0001	78	0.4094	0.5	1.387	1.5	0.2	80	536	6.9	3939 ± 9	1.100	3.4	1.102	3.4	0.4081	0.6
69-2	0.0002	35	0.4073	0.5	1.356	0.9	0.4	84	553	6.8	3928 ± 9	1.098	3.7	1.102	3.7	0.4051	0.6
53-1	0.0001	39	0.4030	0.4	0.913	0.8	0.2	128	566	4.6	3916 ± 6	1.090	3.4	1.092	3.4	0.4020	0.4
71-1	0.0003	28	0.4076	0.4	0.771	0.5	0.5	148	552	3.8	3927 ± 6	1.092	3.4	1.097	3.4	0.4048	0.4
13-1	0.0011	22	0.4175	1.2	3.696	1.1	1.6	35	584	17.3	3938 ± 20	0.941	3.7	0.957	3.7	0.4078	1.4
37-1	0.0004	16	0.4082	0.4	0.970	0.6	0.6	142	635	4.6	3927 ± 7	1.076	4.3	1.083	4.3	0.4047	0.4
14303,52																	
1-1	0.0104	13	0.4886	2.2	2.429	1.1	18.9	102	1839	8.5	3907 ± 61	0.786	8.9	0.969	9.4	0.3993	8.0
2-1	0.0130	15	0.5060	3.0	2.481	1.3	23.6	51	990	9.2	3883 ± 95	0.821	5.6	1.074	7.4	0.3931	12.6
2-2	0.0119	12	0.4912	2.0	2.625	1.5	21.5	48	1051	10.4	3859 ± 64	0.829	3.9	1.057	5.1	0.3869	8.5
2-3	0.0128	14	0.5031	2.2	2.572	1.3	23.3	48	1009	9.9	3877 ± 83	0.866	5.6	1.129	7.0	0.3916	11.0
3-1	0.0131	12	0.5098	2.4	0.633	7.5	23.7	212	342	0.8	3899 ± 72	0.938	7.3	1.230	8.2	0.3974	9.6
4-1	0.0087	11	0.4704	1.9	2.223	1.1	15.8	64	1111	8.2	3890 ± 43	0.954	2.8	1.133	3.5	0.3950	5.7
4-2	0.0403	7	0.7251	2.6	2.090	0.9	73.1	49	857	8.2	3607 ± 430	0.276	16.9	1.025	24.8	0.3278	56.4
4-3	0.0112	26	0.4912	3.9	2.050	1.3	20.4	60	953	7.5	3886 ± 130	0.828	8.3	1.040	10.6	0.3938	17.3
4-4	0.0170	6	0.5364	1.5	1.896	1.4	30.9	59	844	6.8	3859 ± 58	0.748	3.0	1.082	4.2	0.3868	7.7
4-5	0.0288	10	0.6302	3.2	1.887	1.2	52.2	50	665	6.3	3777 ± 226	0.604	7.9	1.264	13.2	0.3666	29.7
5-1	0.0072	18	0.4581	2.8	2.764	1.2	13.0	34	760	10.6	3895 ± 57	0.849	3.9	0.976	4.7	0.3964	7.6
5-2	0.0123	12	0.4968	1.8	2.366	1.2	22.3	35	647	8.7	3867 ± 66	0.827	3.7	1.065	5.0	0.3890	8.8
5-3	0.0144	9	0.5142	1.4	2.728	1.5	26.1	30	686	10.7	3863 ± 65	0.800	3.7	1.083	5.0	0.3880	8.6
5-4	0.0155	12	0.5249	2.1	2.568	1.4	28.1	29	603	9.9	3868 ± 90	0.723	5.5	1.006	7.1	0.3893	11.9
5-5	0.0184	10	0.5432	2.1	2.049	1.7	33.5	42	590	6.7	3823 ± 102	0.639	3.6	0.961	6.2	0.3779	13.4
6-1	0.0229	4	0.5794	1.5	1.880	1.4	41.6	61	808	6.2	3796 ± 62	0.527	12.4	0.903	12.7	0.3711	8.2
6-2	0.0202	13	0.5617	3.8	2.370	1.5	36.7	52	973	8.9	3840 ± 158	0.539	10.7	0.851	13.1	0.3821	21.0
7-1	0.0172	6	0.5311	1.2	2.190	1.0	31.3	47	779	7.9	3815 ± 55	0.706	5.4	1.028	6.1	0.3759	7.3
7-2	0.0112	10	0.4806	1.5	2.203	1.1	20.3	42	714	8.0	3836 ± 54	0.835	3.4	1.048	4.3	0.3811	7.1
7-3	0.0118	13	0.4960	2.4	2.219	1.4	21.4	38	645	7.9	3885 ± 70	0.916	2.7	1.166	4.4	0.3937	9.3
7-4	0.0136	6	0.5063	1.2	2.084	1.2	24.7	38	586	7.3	3857 ± 38	0.789	3.1	1.048	3.6	0.3864	5.0
7-5	0.0120	9	0.4799	2.1	2.019	1.3	21.8	38	577	7.2	3794 ± 55	0.784	3.5	1.003	4.3	0.3706	7.3
8-1	0.0341	7	0.6717	2.6	2.137	0.9	61.9	59	984	7.8	3694 ± 260	0.314	6.1	0.825	13.1	0.3470	34.1
14321,16																	
1-1	0.0022	22	0.4297	1.0	1.812	0.7	4.0	57	562	10.1	3951 ± 18	0.928	4.4	0.966	4.5	0.4113	2.4
2-1	0.0124	14	0.5114	2.7	1.919	0.6	22.5	48	460	9.9	3936 ± 78	0.760	6.5	0.980	7.6	0.4072	10.4
3-1	0.0333	11	0.6878	2.1	2.915	2.5	60.5	10	81	8.0	3936 ± 178	0.302	15.5	0.764	18.1	0.4072	23.7
4-1	0.0276	14	0.6419	1.3	2.540	0.6	50.1	27	246	9.4	3951 ± 74	0.541	5.6	1.085	6.8	0.4114	9.9
5-1	0.0152	15	0.5380	1.4	2.743	0.5	27.6	26	248	10.0	3949 ± 41	0.802	4.5	1.108	5.0	0.4108	5.5
6-1	0.0230	12	0.5950	3.8	3.172	2.8	41.9	15	148	10.3	3894 ± 172	0.564	13.2	0.970	15.7	0.3960	22.8
7-1	0.0210	13	0.5950	3.6	3.630	2.6	38.2	13	142	11.4	3997 ± 149	0.565	12.2	0.915	14.6	0.4242	19.9

Table 2. *Continued.* U-Pb data for the apatite and zircon grains from Apollo 14 breccia thin sections.

Sample	$^{204}Pb/^{206}Pb$	%err	$^{207}Pb/^{206}Pb$	%err	$^{208}Pb/^{206}Pb$	%err	%com Pb^b	U (ppm)	Th (ppm)	Th/U	$^{207}Pb/^{206}Pb$ age	$^{238}U/^{206}Pb$	%err	$^{238}U/^{206}Pb^c$	%err	$^{207}Pb^*/^{206}Pb^*$	%err
Zircon																	
14306,60																	
74-1	0.00111	29	0.491	0.7	0.181	5.7	2.0	43	24	0.59	4191±12	1.042	3.1	1.064	3.2	0.4831	0.9
93-1	0.00049	42	0.493	0.9	0.176	2.2	0.9	28	17	0.63	4210±14	1.094	3.5	1.104	3.5	0.4897	0.9
75-1	0.00051	62	0.491	0.6	0.194	3.1	0.9	49	33	0.71	4204±12	1.089	3.0	1.100	3.1	0.4876	0.8
72-1	0.00383	23	0.512	0.8	0.287	10.0	7.0	32	19	0.62	4196±25	0.990	3.3	1.063	3.8	0.4850	1.6
67-1	0.01329	27	0.570	2.4	0.539	18.4	24.1	12	4	0.36	4161±120	0.860	4.7	1.134	9.8	0.4735	8.1
19-1	0.00015	105	0.487	0.8	0.127	2.2	0.3	37	17	0.49	4200±12	1.047	3.3	1.050	3.3	0.4861	0.8
57-1	0.00090	49	0.494	0.8	0.172	2.2	1.6	37	22	0.61	4204±16	1.078	3.4	1.095	3.5	0.4874	1.0
14066,47																	
63-1	0.00204	21	0.492	0.9	0.149	2.9	3.7	28	12	0.45	4174±18	0.984	7.0	1.022	7.1	0.4776	1.2
48-1	0.00009	56	0.540	0.5	0.137	1.2	0.2	135	69	0.53	4352±6	0.984	6.8	0.986	6.8	0.5392	0.5
42-1	0.00051	36	0.498	1.1	0.094	2.5	0.9	43	14	0.34	4225±18	1.061	6.9	1.070	6.9	0.4946	1.2
32-1	0.00018	54	0.475	0.5	0.113	2.6	0.3	139	55	0.41	4162±8	1.064	6.8	1.067	6.8	0.4737	0.5
33-1	0.00047	33	0.474	0.4	0.161	2.9	0.9	298	168	0.58	4153±6	1.010	6.8	1.019	6.8	0.4709	0.5
14303,52																	
1-1	0.00029	37	0.428	1.0	0.179	2.0	0.6	41	27	0.76	4002±8	1.011	2.4	1.016	2.4	0.4256	1.1
2-1	0.00024	11	0.534	0.3	0.346	0.5	0.5	305	418	1.49	4335±2	0.948	2.4	0.952	2.4	0.5328	0.3
3-1	0.00018	32	0.526	3.9	0.203	2.4	0.3	62	47	0.79	4313±29	1.044	2.1	1.048	2.1	0.5248	4.0
3-2	0.00486	9	0.497	2.2	0.305	4.7	9.1	61	29	0.50	4121±21	1.046	2.2	1.147	2.5	0.4610	2.8
4-1	0.00024	20	0.491	0.5	0.179	1.0	0.4	164	111	0.69	4208±4	1.068	2.1	1.073	2.2	0.4890	0.5
4-2	0.00328	19	0.509	0.8	0.288	7.3	6.1	134	93	0.71	4201±12	0.985	2.1	1.047	2.6	0.4864	1.6
5-1	0.00055	17	0.526	0.9	0.136	1.9	1.0	47	23	0.47	4306±7	1.030	2.3	1.040	2.3	0.5223	0.9
5-2	0.00043	17	0.533	0.8	0.133	1.6	0.8	68	33	0.49	4327±6	0.994	2.3	1.002	2.3	0.5301	0.8
5-3	0.00055	13	0.539	0.7	0.153	1.5	1.0	76	41	0.54	4342±5	1.015	2.5	1.025	2.5	0.5356	0.7
6-1	0.00018	30	0.529	0.9	0.141	2.0	0.3	44	24	0.55	4320±7	1.027	2.3	1.031	2.3	0.5276	0.9
7-1	0.00342	8	0.493	0.9	0.293	2.6	6.4	88	59	0.72	4145±9	0.986	2.3	1.051	2.4	0.4684	1.2
8-1	0.00448	13	0.489	1.3	0.335	6.9	8.4	76	54	0.68	4103±15	1.060	2.2	1.154	2.6	0.4553	2.0
9-1	0.00827	18	0.542	2.0	0.361	13.4	15.5	61	16	0.20	4194±36	0.894	2.6	1.052	5.6	0.4842	4.9
14321,16																	
1-1	0.00003	34	0.500	0.8	0.230	1.2	0.1	252	216	1.00	4039±12	0.980	2.1	1.068	9.9	0.4363	1.7
2-1	0.00002	44	0.532	0.4	0.123	1.0	0.0	166	82	0.50	3974±76	1.021	2.1	1.141	13.7	0.4176	10.2
2-2	0.00001	55	0.531	0.5	0.135	1.4	0.0	169	90	0.55	4020±6	1.016	2.2	1.109	8.6	0.4308	0.8

[a] All errors are 2-sigma, percent.
[b] Proportion of non-radiogenic Pb.
[c] Radiogenic Pb.

Table 3. Ages of individual apatite grains calculated from the multiple ion probe analyses.

Sample/grain	3D-concordia intercept age	$^{207}Pb/^{204}Pb–^{206}Pb^{204}Pb$ isochron age	Weighted average $^{207}Pb^*/^{206}Pb^*$ age
14306-32	3911 ± 290 Ma	3950 ± 180 Ma	3898 ± 58 Ma
14306-56	3901 ± 140 Ma	3931 ± 110 Ma	3892 ± 60 Ma
14306-71	3955 ± 150 Ma	3964 ± 140 Ma	3912 ± 34 Ma
14306-7	3794 ± 810 Ma	3921 ± 90 Ma	3906 ± 42 Ma
14306-73	3844 ± 250 Ma	3954 ± 36 Ma	3940 ± 24 Ma
14303-2	3615 ± 2800 Ma	3660 ± 1500 Ma	3869 ± 44 Ma
14303-5	3908 ± 150 Ma	3909 ± 58 Ma	3876 ± 32 Ma
14303-6	3919 ± 340 Ma	3920 ± 100 Ma	3871 ± 31 Ma
14303-9	3879 ± 360 Ma	3851 ± 130 Ma	3838 ± 39 Ma

section 14321,16 (Fig. 8). Zircon grains are 30–40 microns in size and imaging made after ion probe analysis revealed that only one spot was placed entirely within the zircon. The other two spots have a small overlap with the surrounding plagioclase grains. As a result, these two analyses show a high proportion of ^{204}Pb with $^{206}Pb/^{204}Pb$ ratios of 48 and 127, respectively. The third analysis has higher $^{206}Pb/^{204}Pb$ of 1804. Nevertheless, when corrected for common Pb all analyses fall within a limited $^{207}Pb/^{206}Pb$ age range (Table 2) with an average of 4023 ± 24 Ma. This is interpreted as the best estimate of the crystallization age of the anorthosite.

Seven analyses of five 30–50 micron apatite grains show variation of U concentration between 10 and 57 ppm and consistent Th/U between 8 and 11.4. One apatite analysis has a relatively high $^{206}Pb/^{204}Pb$ of 454 whereas the others range from 30 to 81, which combined with the small size of these grains highlights once again that an increase in the proportion of ^{204}Pb is associated with the surface contamination of the sample which is more pronounced at the grain boundaries and near the cracks. A line defined by all seven analyses determines 3D-concordia intercept of 3950 ± 84 Ma (Fig. 4), while the $^{204}Pb/^{206}Pb – ^{207}Pb/^{206}Pb$ isochron age is 3951 ± 22 Ma (Fig. 5) and the weighted average of the common Pb corrected $^{207}Pb/^{206}Pb$ ages is 3950 ± 15 Ma. The last two are slightly younger than the age of anorthosite, indicating that the apatite was reset by a process similar to that affecting all other analyzed samples.

DISCUSSION

Apatite Analyses

The relatively high proportion of ^{204}Pb in at least two samples (13406, 60 and 14303, 52) makes these samples very sensitive to the correction for initial Pb especially in view of observations suggesting high μ-values are characteristic of lunar rocks (e.g., Meyer et al. 1996). Meyer et al. (1996) used a model where the initial Pb selected for the correction was calculated as a mixture of meteoritic Pb and radiogenic lunar Pb. However, all our apatite data, shown on a $^{207}Pb/^{206}Pb$ versus $^{204}Pb/^{206}Pb$ plot, form a single line (Fig. 9) giving an age of 3927.2 ± 2.8 Ma, with a MSWD of 1.05 and a

probability of fit of 0.36. These MSWD and probability values indicate that the data fall on an isochron within the experimental errors and that the initial Pb composition is similar for all analyses. These data also indicate a single source of a non-radiogenic Pb for all samples. It is likely that this source is terrestrial contamination of the samples during their cutting and polishing as the best fit line passes slightly below modern Stacey and Kramers common Pb on a $^{207}Pb/^{206}Pb$ versus $^{204}Pb/^{206}Pb$ plot and intercepts the terrestrial Pb growth curve at about 4.2 Ga (Stacey and Kramers 1975). However, even a significant variation of the initial Pb composition would result in a very small change in the slope of the line. For example correcting all apatite analyses using common Pb obtained from the analysis of olivine clasts in the sample 14321,16 results in an average $^{207}Pb/^{206}Pb$ age of 3923.2 ± 4.3 Ma with a slight increase of MSWD to 2.4. This age is similar to that obtained from the best fit in the $^{207}Pb/^{206}Pb$ versus $^{204}Pb/^{206}Pb$ coordinates. Alternatively, if all data are corrected for a 3.9 Ga lead calculated from the model assuming Canyon Diablo troilite as a starting composition and selecting $^{238}U/^{204}Pb$ (μ value) to produce the starting composition of Stacey and Kramers at 3.7 Ga, the average $^{207}Pb/^{206}Pb$ age obtained from all apatite analyses is 3926.4 ± 2.3 Ma (MSWD = 2.7).

Alternatively, calculating the best linear fit through the uncorrected data in 3D ($^{204}Pb/^{206}Pb–^{207}Pb/^{206}Pb–^{238}U/^{206}Pb$) system or constraining isochrons in the $^{204}Pb/^{206}Pb–^{207}Pb/^{206}Pb$ plane can help to avoid making a decision with respect to the selection of exact initial Pb composition. Ages calculated from the best fit lines constrained to the nearest concordia intercept in 3D and using all analytical points for individual samples as well as the best fit lines constrained using $^{204}Pb/^{206}Pb–^{207}Pb/^{206}Pb$ data are similar within the errors (Figs. 10 a, 10b). This suggests that apatite grains have experienced a complete loss of radiogenic Pb in all samples at the same time around 3.92 Ga, which is attributed to the extreme pressure and temperature spike associated with breccia formation during the Imbrium impact. The best estimate of the time of this impact can be obtained by combining U-Pb apatite data for all analyzed samples. When some of the most common Pb rich analyzed ($^{206}Pb/^{204}Pb$ less than 100) are excluded from the calculations, the 3D ($^{204}Pb/$
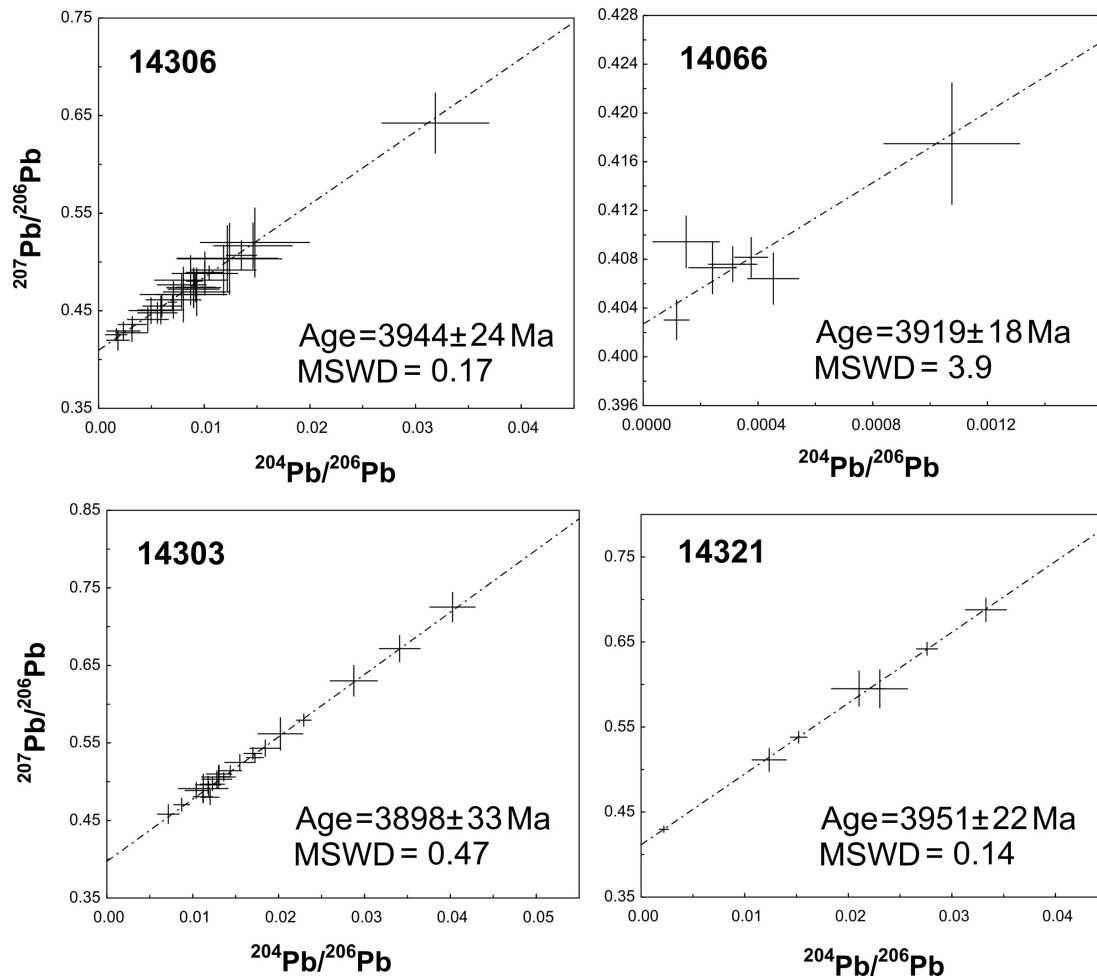
Fig. 5. $^{207}Pb/^{206}Pb$–$^{204}Pb/^{206}Pb$ isochrons for analyzed apatite in the 4 breccia samples.

^{206}Pb–$^{207}Pb/^{206}Pb$–$^{238}U/^{206}Pb$) line and $^{204}Pb/^{206}Pb$–$^{207}Pb/$ ^{206}Pb isochron constrained using uncorrected data as well as the $^{207}Pb/^{206}Pb$ data corrected for the common Pb obtained from the olivine analyses define exactly the same age (Figs. 10a–c). The $^{204}Pb/^{206}Pb$–$^{207}Pb/^{206}Pb$ isochron is least affected by the uncertainties associated with the common Pb correction and ion probe fractionation of U/Pb ratios. Therefore, the 3926 ± 3 Ma age determined from this isochron is the best estimate of the time of impact associated resetting of the U-Pb system in apatite.

Comparison with Zircon U-Pb Ages

U-Pb ages of zircon in the breccias are all significantly older than the age of 3926 ± 3 Ma of coexisting apatites. In addition the ages of zircons in the breccia matrices show a considerable variation suggesting that other minerals in the breccias have parent rocks covering a wide range of ages. The zircon age of the norite clast of 4201 ± 6 Ma (breccia 14306,60) dates the norite and the cogenetic apatite, clearly demonstrating that the apatite age has been reset as a
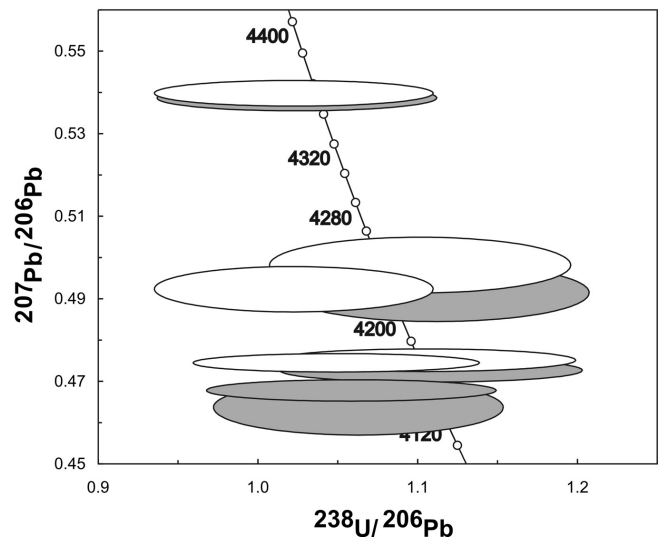
Fig. 6. Tera-Wasserburg concordia diagram showing analyses of zircon grains from thin section 14066,47 (open ellipses—common Pb uncorrected data; grey ellipses—corrected for the common Pb obtained from the analysis of olivine).
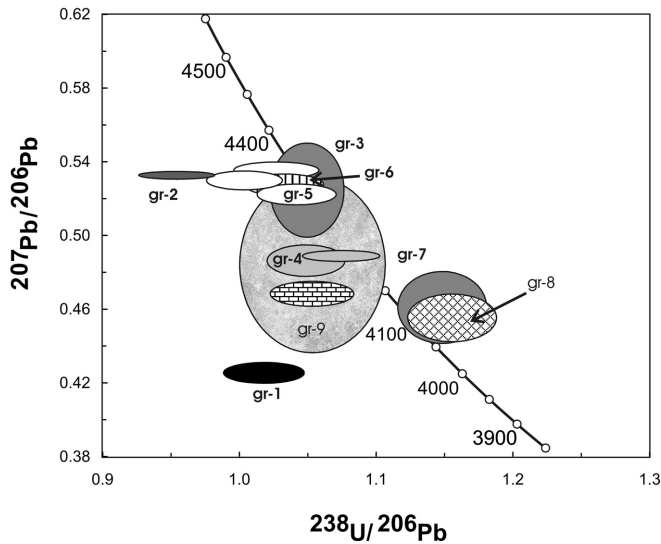
Fig. 7. Tera-Wasserburg concordia diagram showing 13 common Pb uncorrected analyses of nine zircon grains from the thin section 14303,52. The older group is composed of zircon grains -2, -5, -6 and one analysis of grain-3, and the younger group is composed of grains -4, -7, -8, -9 and the second analyse of grain-3. Each different pattern filling the ellipses correspond to a different zircon grain, identified as gr-#.

consequence of heating during the Imbrium impact. Similarly the age of zircon of 4023 ± 24 Ma in the anorthosite clast in sample 14321,16 dates both the anorthosite and cogenetic apatite. The U-Pb system of zircon shows no evidence of isotopic disturbance during this event. This conclusion is supported by the absence of ca. 3.9 Ga ages in the overall population of zircons analyzed in lunar samples (Meyer et al. 1996; Nemchin et al. 2008). A rare exception is the group of grains investigated by Gnos et al. (2004) in the impact melt preserved in the lunar meteorite Sayh al Uhaymir (SAU) 169. This group defined an average ^{207}Pb/^{206}Pb age of 3909 ± 13 Ma. Additional zircon grains from the same meteorite were analyzed by Liu et al. (2009) who reported an average of 3918 ± 9 Ma. Both zircon ages are similar to the age 3926 ± 3 Ma determined for the apatite grains in Apollo 14 breccias.

The Age of Imbrium Impact

A narrow range of Rb-Sr and Ar-Ar ages of 3.79 to 3.90 Ga has been reported for a variety of rocks, minerals and breccia matrices from Apollo 14 (as summarized by Wilhelms 1987). This suggests that the Ar-Ar and Rb-Sr ages are independent of the nature of the sample, i.e., all samples behave as though the Ar-Ar and Rb-Sr systems of all breccia fragments, matrices and analyzed mineral clasts have been completely reset at some time within this time interval. Based on these data the most recently proposed age for the Imbrium impact is defined as 3.85 ± 0.02 Ma (Wilhelms 1987; Ryder 1990, 1994; Spudis 1993; Hartmann et al. 2000; Stöffler and Ryder
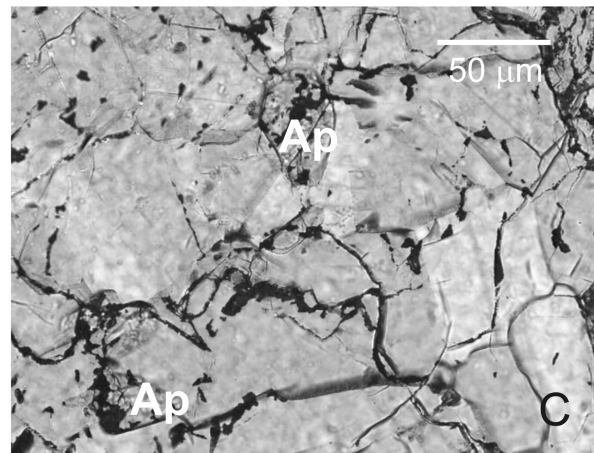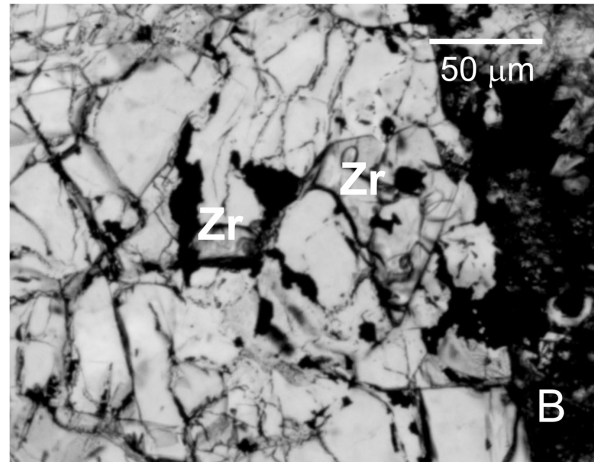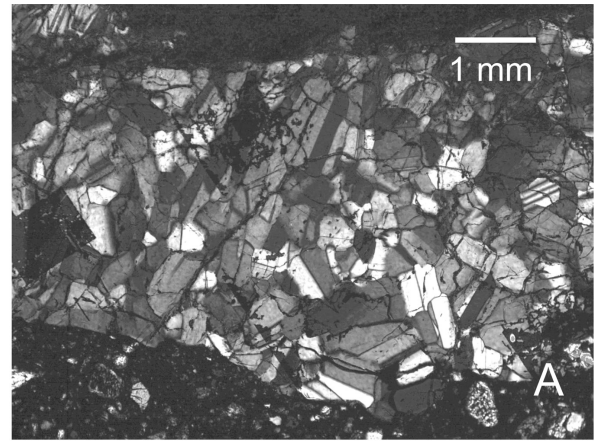
Fig. 8. Analyzed zircon and apatite grains from the anorthosite clast in breccia thin section 14321,16. a) Anorthosite clast (crossed polars). b) Zircon (Zr). c) Apatite (Ap) crystals surrounded by plagioclase grains (plane polarized light).

2001). This age is clearly younger than both 3909 ± 13 Ma and 3926 ± 3 Ma suggested, respectively, by zircon (Gnos et al. 2004) and apatite data (this work). However, recalculation of Ar-Ar age using decay constant suggested by Min et al. (2000) will result in about 1% increase in the Ar-Ar age, making it similar within the errors to the age estimated
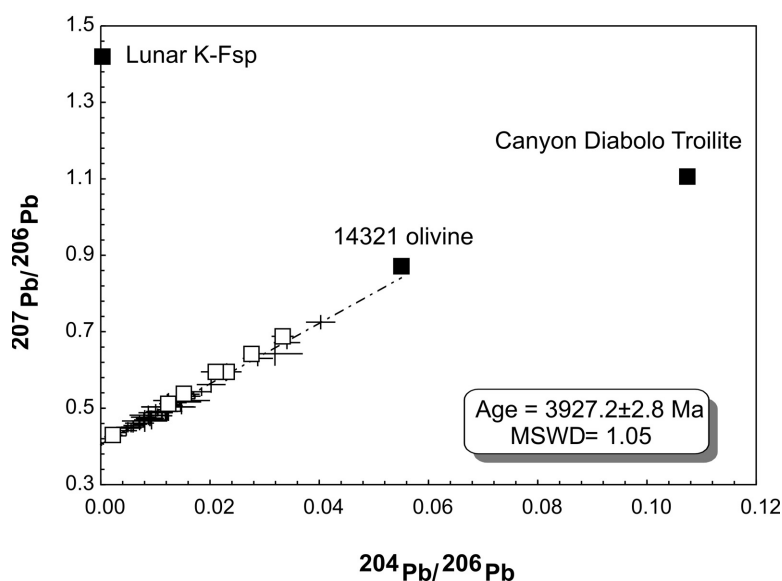
Fig. 9. Combined $^{207}Pb/^{206}Pb$–$^{204}Pb/^{206}Pb$ apatite data shown relative to different sources of initial Pb.

from the zircon (Gnos et al. 2004) and apatite analyses. Nevertheless, this recalculation does not solve a discrepancy between U-Pb and Rb-Sr data. The Rb-Sr ages of basaltic clasts from Apollo 14 breccias presented by Papanastassiou and Wasserburg (1971) are similar within the errors to the U-Pb apatite age. However, these Rb-Sr ages were calculated with a Rb decay constant that is now considered inaccurate. When recalculated with the currently accepted decay constant value (Steiger and Jäger 1977) these ages become significantly younger that those determined from apatite U-Pb systems. The observed discrepancies highlight that the precise and accurate chronology of lunar impact history requires reconciliation of different isotopic systems, especially if a significant number of major impacts is predicted to occur in a very short period of time according to the model of Late Heavy Bombardment. Consequently, current apatite results can be viewed only as providing U-Pb age of Fra Mauro Formation. Following widely accepted interpretation that this formation represents Imbrium ejecta the apatite data also determine U-Pb age of Imbrium impact.

Thermal History of Breccias at the Apollo 14 Landing Site

Considering that both apatite and zircon grains in the studied breccia samples are mineral clasts that originally crystallized in the rocks predating breccia formation, the thermal history of the breccias from the Apollo 14 landing site in the aftermath of the Imbrium impact can be evaluated on the basis of observed U-Pb resetting patterns of apatite and zircon and Pb diffusion data available for these two minerals (Cherniak et al. 1991; Cherniak and Watson 2001). The Pb diffusion parameters of apatite and zircon are very different, therefore, the observed difference in the behavior of U-Pb systems in these minerals found in the same thin sections of

lunar breccia can constrain the cooling history of the samples and the ejecta blanket. The process can be modeled assuming a specific thickness of the ejecta blanket (l) and an initial temperature (T_o). Setting temperature at the surface to 0 °C for any time (t), the question of ejecta cooling is reduced to a one dimensional conductivity problem in semi-infinite half-space, with the initial conditions $T(0 < d \leq l) = T_o$ and $T(l < d) = 0$. This problem has a standard analytical solution (e.g., Carslaw and Jager 1959):

$$T = \frac{To}{2}\left\{ 2Erf\left(\frac{d}{2\sqrt{kt}}\right) - Erf\left(\frac{d-1}{2\sqrt{kt}}\right) - Erf\left(\frac{d+1}{2\sqrt{kt}}\right)\right\} \quad (1)$$

where k is thermal diffusivity.

Equation 1 defines the temperature at any time and at any depth within the cooling ejecta blanket. Diffusion of Pb from apatite and zircon can be modeled, assuming a specific depth (d) within the ejecta blanket. The temperature decrease for this depth calculated from Equation 1 is translated into the change of the diffusion coefficient D ($D = D_oExp[-E/RT]$) in the mass diffusion equation, which for a spherical geometry of the grains, assuming homogenous, isotropic diffusion and no boundary effects, can be written as:

$$\frac{\partial C}{\partial t} = \frac{\partial}{\partial_r}\left(D\frac{\partial C}{\partial_r}\right) + \frac{2}{r}D\frac{\partial C}{\partial_r} \quad (2)$$

where C is Pb concentration and r is a radial coordinate (i.e., distance from the centre of the sphere).

Equation 2 was solved numerically using the Crank-Nicholson finite difference scheme based on a published solution for Ar diffusion (e.g., Wheeler 1996). The model has been applied to a range of sample depths (d) and initial temperature of the ejecta blanket (T_o). The thickness of the
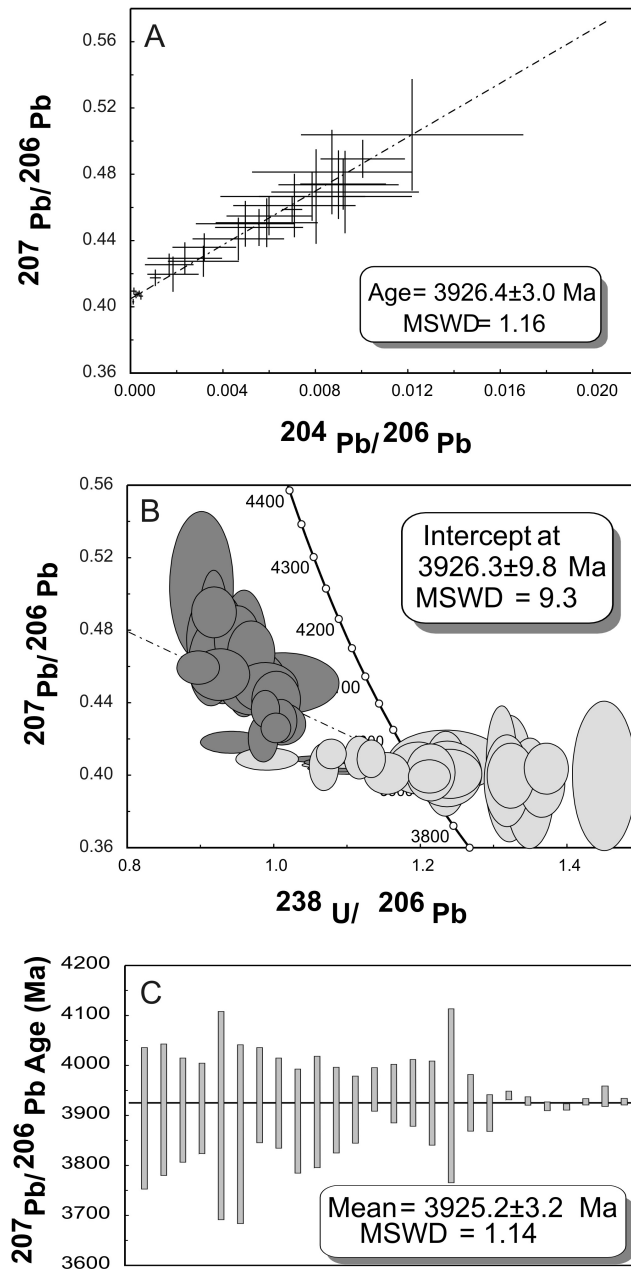
Fig. 10. Combined ages determined from the most radiogenic Pb data for the apatite grains. a) $^{207}Pb/^{206}Pb$ – $^{204}Pb/^{206}Pb$ isochron. b) Best fit in the 3D $^{207}Pb/^{206}Pb$–$^{204}Pb/^{206}Pb$–$^{238}U/^{206}Pb$ system. c) Weighted average of olivine-Pb corrected $^{207}Pb/^{206}Pb$ ages. Both (a) and (b) show data uncorrected for common Pb and excluding values with $^{206}Pb/^{204}Pb < 100$.

blanket (*l*) was fixed at 200 m based on the estimated thickness of Fra Mauro Formation of Eggleton and Offield (1970). However, this parameter has only minor influence on the calculated diffusion behavior of Pb, especially considering that the studied samples are expected to cool at relatively shallow levels within the ejecta blanket from where they were delivered to the surface during excavation subsequent to the cooling. This relatively shallow original position of the samples is dictated by the lower probability of sample delivery to the surface (where they were collected)

from deeper stratigraphic levels, unless all Apollo 14 samples represent material ejected from the Cone crater. The apatite and zircon grains were assumed to be 100 and 30 μm in diameter respectively, based on the largest apatite and smallest zircon analyzed in the breccia samples. It was further assumed that if 95% of Pb is lost from the apatite grains, the residual 5% would be impossible to detect as it would result in a change of $^{207}Pb/^{206}Pb$ age by about 15–20 Ma, which is within the average scatter of U-Pb analyses of individual spots in the apatite and zircon. Similarly it will be difficult to
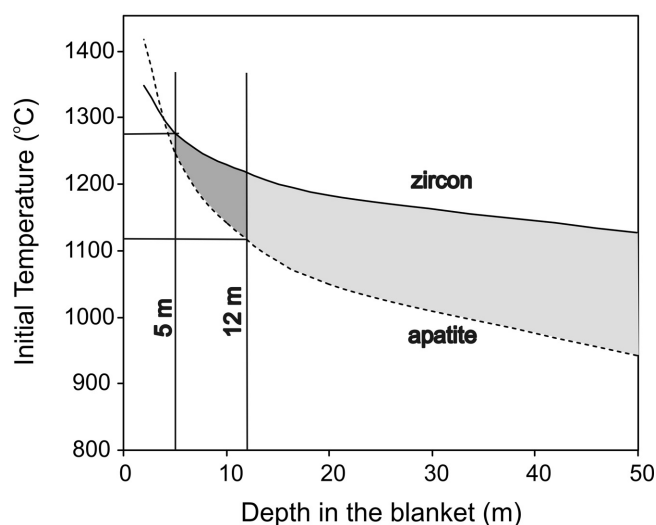
Fig. 11. Temperature and depth constraints for the resetting U-Pb systems in zircon and apatite. The curves indicate possible *T-d* conditions required to allow diffusion of Pb in a 30 μm zircon and 100 μm apatite. The zone between the curves corresponds to the conditions required to allow complete resetting of U-Pb in apatite and no resetting of this system in zircon.

detect a 5% loss of Pb from the zircon. Therefore, calculations were made to determine limits T_o and d fitting the requirements of 95% loss of Pb from the apatite and the absence of more than 5% Pb loss from zircon. The results of these calculations are shown in Fig. 11 as two curves bounding the behavior of Pb in apatite and zircon. Area above the apatite curve represents T_o and d where the apatite will lose more than 95% of the accumulated Pb, whereas the area below the zircon curve represents T_o and d where zircon will retain more than 95% of the accumulated Pb. The area between two curves represents a set of parameters where the resetting of U-Pb system of 100 μm apatite is possible without resetting this system in 30 μm zircon.

The first important implication of the model predictions is that the initial temperature of the blanket cannot exceed 1300 °C, which corresponds to the shallowest possible position of the samples at about 3.5–4 m below the surface. However, at this depth and temperature the field between the apatite and zircon curves is very narrow indicating a very restricted set of possible conditions. Therefore, while this combination of temperature and depth is not impossible, it is highly unlikely that the strict set of conditions can be maintained for the numerous samples collected in the different locations within the landing site. On the other hand, if the samples are located deep within the impact ejecta sheet the probability of their excavation and delivery to the surface is significantly reduced, which is important as all Apollo 14 samples where apatite and zircon were analyzed so far show similar patterns of resetting of U-Pb system and therefore have been under a similar range of thermal conditions. The temperature conditions can be further restricted by the assumption that the

analyzed breccia samples came from the level directly under the regolith and that the regolith thickness reflects the original extension of the ejecta blanket. This thickness at the Apollo 14 landing site is estimated between 5 and 12 m (e.g., Eggleton and Offield 1970), which restricts the initial temperature range for the ejecta blanket to about 1280–1120 °C (Fig. 11). The diffusion behavior of Pb in apatite and zircon in a sample at 9 m depth and an initial temperature of the blanket of 1200 °C is illustrated in Fig. 12. Under these conditions the temperature of the sample will decrease to about 500 °C within the first 4 years of cooling (Fig. 12 a). At this temperature both apatite and zircon should be effectively closed for Pb diffusion. However, after about 5–6 months the amount of Pb left in the entire apatite grain is far beyond the limit that can be detected from the variation of $^{207}Pb/^{206}Pb$ ages (Figs. 12b, c). During the same time interval the temperature decreases to a level lower than the closure temperature of the U-Pb system in zircon which results in a very small proportion of Pb loss from the outer 1 μm layer in the zircon grain, while the rest of the grain is completely unchanged (Figs. 12d–e).

Alternatively, the observed similarity of thermal history shown by different samples can be explained by the initial temperature of the blanket in the range between about 1150 and 1100 °C. For example, if the initial temperature is 1150 °C (Fig. 11), U-Pb systems of apatite grains in samples located between about 10 and 40 m will be completely reset, while zircon will not show any significant Pb-loss. At 1100 °C zircon grains will preserve their original isotopic signatures even at 75 m, estimated depth of the Cone crater. The excavation depth of the samples is unlikely to be significantly lower than the depth of the Cone crater, as a deeper location would require initial temperature of the ejecta blanket to be lower than the solidus of dry basalt, which would contradict the wide occurrence of impact melts in the breccia samples.

Results of diffusion modelling of Pb in zircon and apatite from Apollo 14 breccias find an additional support in the textural characteristics of studied breccia samples. Simonds et al. (1976) modelled thermal equilibration of mixtures of initially cold clasts and impact melts and predicted temperatures attained by the breccia samples with different petrographic characteristics. Their models suggest that the crystalline impact melt breccias such as investigated here samples from Apollo 14 collection, will equilibrate at the temperature in the range of 1400–1000 °C. This is similar to the predictions made on the basis of Pb diffusion in apatite and zircon.

CONCLUSIONS

SIMS measurements on cogenetic zircon and apatite show that the significantly younger apatite grains have been isotopically reset during an event at 3926 ± 3 Ma. Multiple SIMS measurements on individual apatite grains failed to
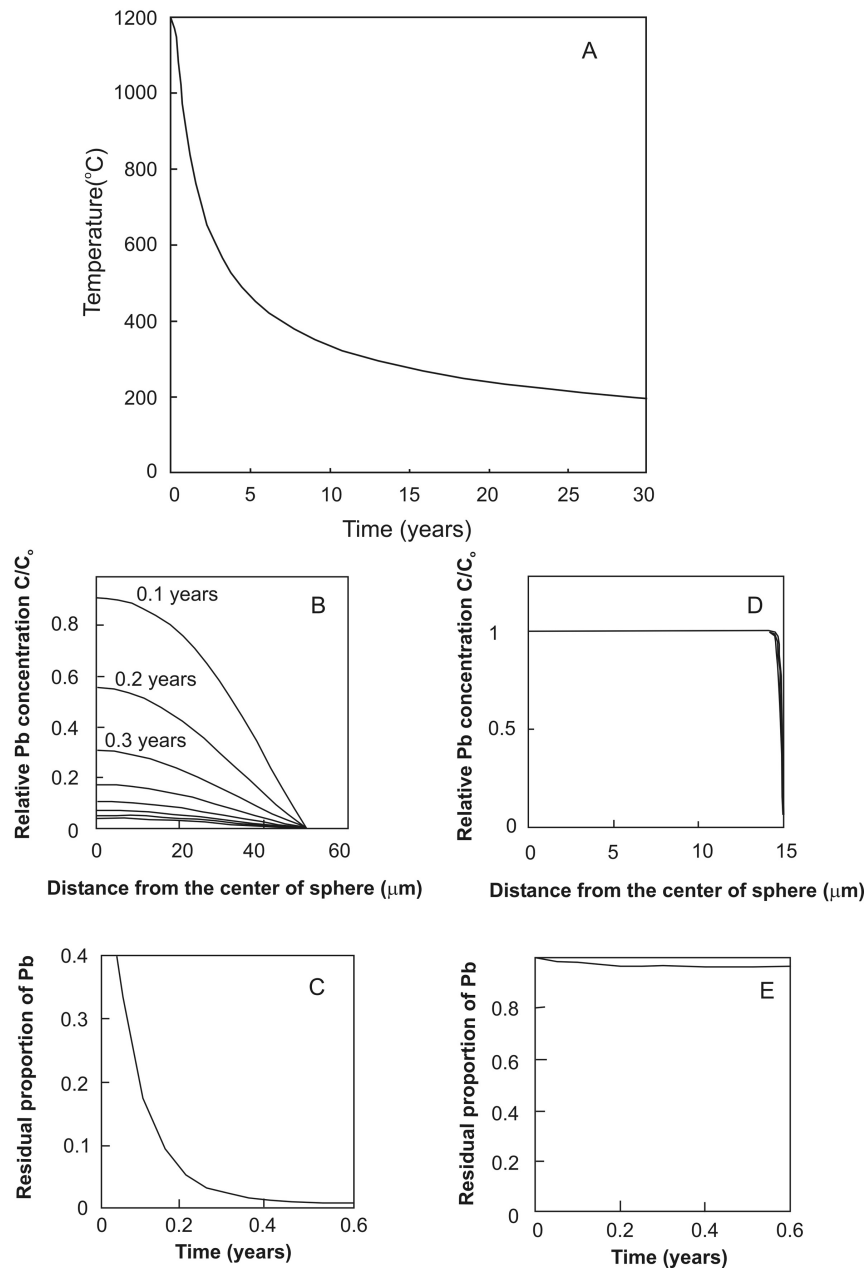
Fig. 12. Cooling history and Pb diffusion in zircon and apatite at the starting temperature (T_o) of 1200 °C and sample depth of 9 m. a) Cooling of the sample during the 30 years since the formation of the ejecta blanket. b) Pb distribution profile across an apatite sphere of 50 μm radius. c) Proportion of Pb left in the apatite sphere versus time. d) Pb distribution profile across a zircon sphere of 15 μm radius. e) Proportion of Pb left in the zircon sphere versus time.

identify any memory of older radiogenic Pb, although the primary apatite ages, as determined from SIMS U-Pb age on cogenetic zircon, were at least 100 Ma older. Moreover, the uniformity of the apatite ages for breccia samples from all parts of the Apollo 14 traversed area suggests that the breccia samples derived from the same source, interpreted to be the underlying Fra Mauro Formation. The widespread response of apatite to conditions existing during the deposition of the Fra Mauro Formation demonstrates the value of apatite in lunar chronology as it has enabled us to date this unit. The

open system behavior of the apatite contrasts with that of the zircon which shows no indication of having been isotopically disturbed during the 3926 Ma event. This contrasting behavior places constraints on the thermal conditions of formation and we conclude, from a consideration of the Pb diffusion parameters of these minerals, that in the vicinity of Cone crater and the Apollo 14 landing site the Fra Mauro Formation was deposited 3926 ± 3 Myr ago at a temperature between 1300 and 1100 °C and cooled down within a few years.

REFERENCES

Alexander E. C. and Davis P. K. 1974. ^{40}Ar-^{39}Ar ages and trace element contents of Apollo 14 breccias: An interlaboratory cross-calibration of ^{40}Ar-^{39}Ar standards. *Geochimica et Cosmochimica Acta* 38:911–928.

Carlson I. C. and Walton W. J. A. 1978. Apollo 14 rock samples. Curators Office. JSC 14240.

Carslaw H. S. and Jaeger J. C. 1959. Conduction of heat in solids, Oxford: Clarendon. 510 p.

Chamberlain K. R. and Bowring S. A. 2000. Apatite-feldspar U-Pb thermochronometer: A reliable, mid-range (~450 °C), diffusion-controlled system, *Chemical Geology* 172:73–200.

Cherniak D. J. and Watson E. B. 2001. Pb Diffusion in zircon, *Chemical Geology* 172:5–24.

Cherniak D. J., Lanford W. A., and Ryerson F. J. 1991. Lead diffusion in apatite and zircon using ion implantation and Rutherford backscattering techniques. *Geochimica et Cosmochimica Acta* 55:1663–1673.

Compston W., Vernon M. J., Berry H., Rudowski R., Gray C. M., Ware N., Chappell B. W., and Kaye M. 1972. Apollo 14 mineral ages and the thermal history of the Fra Mauro formation. Proceedings, 3rd Lunar Science Conference. pp. 1487–1501.

Compston W., Williams I. S., and Meyer C. 1984. U-Pb geochronology of zircons from lunar breccia 73217 using a sensitive high mass-resolution ion microprobe. Proceedings, 14th Lunar and Planetary Science Conference. *Journal of Geophysical Research* 89:B525–B534.

Compston W., Williams I. S., and Meyer C. 1984. Age and chemistry of zircon from late-stage lunar differentiates. 15th Lunar and Planetary Science Conference. pp. 182–183.

Compston W., Williams I. S., and Meyer C. 1991. Initial Pb isotopic compositions of lunar granites as determined by ion microprobe. *In stable isotope geochemistry: A tribute to Samual Epstein.* Geochemical Society Special Publication no. 3. pp. 473–486.

Eggleton R. E. and Offield T. W. 1970. Geologic maps of the Fra Mauro region of the Moon: Apollo 14 pre-mission maps. U.S. Geological Survey Map 1–708.

Gale N. H. 1972. Uranium-lead systematics in lunar basalts. *Earth and Planetary Science Letters* 17:65–78.

Gnos E., Hofmann B. A., Al-Kathiri A., Lorenzetti S., Eugster O., Whitehouse M. J., Villa I. M., Jull A. J. T. 2004. Pinpointing the source of a lunar meteorite: Implications for the evolution of the Moon. *Science* 305:657–659.

Hartmann W. K., Ryder G., Dones L., Grinspoon D. 2000. The time-dependent intense bombardment of the primordial Earth/Moon system. In *The origin of the Earth and Moon*, edited by Canup R. M. and Righter K. Tucson: The University of Arizona Press. pp. 93–512.

Hiesinger H. and Head J. W. 2006. New views of lunar geoscience: An introduction and overview. In *New views of the Moon.* Reviews in Mineralogy and Geochemistry, vol. 60. Mineralogical Society of America. pp. 1–81.

Kennedy A. K. and de Laeter J. R. 1994. The performance characteristics of the WA SHRIMP II ion microprobe. In *8th International Conference on Geochronology, Cosmochronology and Isotope Geology, Berkeley.* USGS Circular 1107. p. 166.

Kirsten T., Deubner J., Horn P., Kaneoka I., Kiko J., Schaeffer O. A., and Thio S. K. 1972. The rare gas record of Apollo 14 and 15 samples. Proceedings, 3rd Lunar Science Conference. pp. 1865–1889.

Krogstad E. J. and Walker R. J. 1994. Higher closure temperatures of the U-Pb system in large apatites from the Tin Mountain pegmatite, Black Hills, South Dakota, USA. *Geochimica et Cosmochimica Acta* 58:3845–3853.

Liu D., Wan Y., Zhang Y., Dong C., Jolliff B. L., Zeigler R. A., and Korotev R. L. 2009. Age of zircons in the impact-melt breccia in SaU 169 lunar meteorite: Beijing SHRIMP II study (abstract #2499). 40th Lunar and Planetary Science Conference. CD-ROM.

Ludwig K. 2001. Users manual for Squid1.02, Berkeley Geochronology Center Special Publication 1a. 19 p.

Meyer C., Williams I. S., and Compston W. 1996. Uranium-lead ages for lunar zircons: Evidence for a prolonged period of granophyre formation from 4.32 to 3.88 Ga. *Meteoritics & Planetary Science* 31:370–387.

Min K., Mundil R., Renne P. R., and Ludwig K. R. 2000. A test for systematic errors in ^{40}Ar/^{39}Ar geochronology through comparison with U/Pb analysis of a 1.1-Ga rhyolite. *Geochimica et Cosmochimica Acta* 64:73–98.

Nemchin A. A., Pidgeon R. T., Whitehouse M. J., Vaughan J. P., and Meyer C. 2008. SIMS U-Pb study of zircon from Apollo 14 and 17 breccias: Implications for the evolution of lunar KREEP. *Geochimica et Cosmochimica Acta* 72:668–689.

Papanastassiou D. A. and Wasserburg G. J. 1971. Rb-Sr ages of igneous rocks from the Apollo 14 mission and the age of the Fra Mauro Formation. *Earth and Planetary Science Letters* 12:36–48.

Pidgeon R. T., Furfaro D., Kennedy A. K., Nemchin A. A., and van Bronswijk W. 1994. Calibration of zircon standards for the Curtin SHRIMP. In *8th International Conference on Geochronology, Cosmochronology and Isotope Geology.* Berkeley, USGS Circular 1107. p. 251.

Pidgeon R. T., Nemchin A. A., van Bronswijk W., Geisler T., Meyer C., Compston W., and Williams I. 2007. Complex history of a zircon aggregate from lunar breccia 73235. *Geochimica et Cosmochimica Acta* 71:1370–1381.

Ryder G. 1994. Coincidence in time of the Imbrium basin impact and Apollo 15 KREEP volcanic flows: The case for impact-induced volcanism. In *Large meteorite impacts and planetary evolution*, edited by Dressler B. O., Grieve R. A. F., and Sharpton V. L. GSA Special Paper 293. pp. 11–18.

Ryder G. 1990. Lunar samples, lunar accretion and the early bombardment of the moon. *EOS Transactions* 71:313–323.

Simonds C. H., Warner J. L., Phinney W. C., and McGee P. E. 1976. Thermal model for impact melt breccia lithification: Manicouagan and the Moon. Proceedings, 7th Lunar Science Conference. pp. 2509–2528.

Simonds C. H., Phinney W. C., Warner J. L., McGee P. E., Geeslin J., Brown R. W., and Rhodes M. J. 1977. Apollo 14 revisited, or breccias aren't so bad after all. Proceedings, 8th Lunar Science Conference. pp. 1869–1893.

Spudis P. D. 1993. *The geology of multi-ring impact basins.* Cambridge Planetary Science Series, vol. 8. Cambridge University Press. 280 p.

Stacey J. S. and Kramers J. D. 1975. Approximation of terrestrial lead isotope evolution by a two-stage model. *Earth and Planetary Science Letters* 26:207–221.

Steiger R. H. and Jäger E. 1977. Subcommission on geochronology: Convention on the use of decay constants in geo- and cosmochronology. *Earth and Planetary Science Letters* 36:359–362.

Stöffler D. and Ryder G. 2001. Stratigraphy and isotope ages of lunar geologic units: Chronological standard for the inner solar system. In *Chronology and evolution of Mars*, edited by Kallenbach R., Geiss J., Hartmann W. K. Space Science Series of ISSI. Dordrecht: Kluwer Academic Publishers. pp. 9–54.

Swann G. A., Trask N. J., Hait M. H., Sutton R. L. 1971. Geologic setting of the Apollo 14 samples. *Science* 173:716–719.

Tera F. and Wasserburg G. J. 1972. U-Th-Pb systematics in three Apollo 14 basalts and the problem of initial Pb in lunar rocks, *Earth and Planetary Science Letters* 14:281–304.

Terada K. and Sano Y. 2003. In situ U=Pb dating and REE analysis of phosphates in extraterrestrial materials. *Applied Surface Science* 203–204:810–813.

Terada K., Anand M., Sokol A. K., Bischoff A., and Sano Y. 2007. Cryptomare magmatism 4.35 Gyr ago recorded in lunar meteorite Kalahari 009. *Nature* 450:849–852.

Turner G., Huneke J. C., Podosek F. A., and Wasserburg G. J. 1971. ^{40}Ar-^{39}Ar ages and cosmic-ray exposure ages of Apollo 14 samples. *Earth and Planetary Science Letters* 12:19–35.

Turner G., Huneke J. C., Podosek F. A., and Wasserburg G. J. 1972. Ar^{40}-Ar^{39} systematics in rocks and separated minerals from Apollo 14. Proceedings, 3rd Lunar Science Conference. pp. 1589–1612.

Wheeler J. 1996. DIFFFRAG: A program for simulating argon diffusion profiles in minerals. *Computers and Geosciences* 22: 919–929.

Whitehouse M. J. and Kamber B. S. 2005. Assigning dates to thin gneissic veins in high-grade metamorphic terranes: A cautionary tale from Akilia, Southwest Greenland. *Journal of Petrology* 46: 291–318.

Whitehouse M. J., Kamber B. S., and Moorbath S. 1999. Age significance of U–Th–Pb zircon data from early Archaean rocks of west Greenland—a reassessment based on combined ion-microprobe and imaging studies. *Chemical Geology* 160:201–224.

Wilhelms D. E. 1987. The geologic history of the Moon. USGS Professional Paper 1348.

Woodhead J. D. and Hergt J. M. 2000. Pb-isotope analyses of USGS reference materials. *Geostandards Newsletter* 24:33–38.